Redox Biology 46 (2021) 102084

Contents lists available at ScienceDirect

Redox Biology

journal homepage: www.elsevier.com/locate/redox

PARP1 deficiency protects against hyperglycemia-induced neointimal hyperplasia by upregulating TFPI2 activity in diabetic mice

Zhao-yang Wang [a,b,1], Meng-qi Guo [c,1], Qing-ke Cui [d,1], Haitao Yuan [b], Shan-ji Fu [e], Bin Liu [a], Fei Xie [a], Wen Qiao [a], Jie Cheng [a], Ying Wang [a,**], Ming-xiang Zhang [a,*]

[a] Department of Cardiology, Qilu Hospital, Cheeloo College of Medicine, Shandong University, Jinan, Shandong, China
[b] Department of Cardiology, Shandong Provincial Hospital Affiliated to Shandong First Medical University, Jinan, Shandong, China
[c] Department of Cardiology, the Affiliated Hospital of Qingdao University, Qingdao, Shandong, China
[d] Department of Neurosurgery, Liaocheng People's Hospital, Liaocheng, Shandong, China
[e] Department of Clinical Laboratory, Qilu Hospital of Shandong University, Jinan, Shandong, 250012, China

ARTICLE INFO

Keywords:
PARP1
Neointimal hyperplasia
Diabetes
TFPI2

ABSTRACT

Diabetes mellitus (DM) promotes neointimal hyperplasia, characterized by dysregulated proliferation and accumulation of vascular smooth muscle cells (VSMCs), leading to occlusive disorders, such as atherosclerosis and stenosis. Poly (ADP-ribose) polymerase 1 (PARP1), reported as a crucial mediator in tumor proliferation and transformation, has a pivotal role in DM. Nonetheless, the function and potential mechanism of PARP1 in diabetic neointimal hyperplasia remain unclear. In this study, we constructed PARP1 conventional knockout ($PARP1^{-/-}$) mice, and ligation of the left common carotid artery was performed to induce neointimal hyperplasia in Type I diabetes mellitus (T1DM) mouse models. PARP1 expression in the aorta arteries of T1DM mice increased significantly and genetic deletion of PARP1 showed an inhibitory effect on the neointimal hyperplasia. Furthermore, our results revealed that PARP1 enhanced diabetic neointimal hyperplasia via downregulating tissue factor pathway inhibitor (TFPI2), a suppressor of vascular smooth muscle cell proliferation and migration, in which PARP1 acts as a negative transcription factor augmenting TFPI2 promoter DNA methylation. In conclusion, these results suggested that PARP1 accelerates the process of hyperglycemia-induced neointimal hyperplasia via promoting VSMCs proliferation and migration in a TFPI2 dependent manner.

1. Introduction

Accelerated intimal thickening in diabetes mellitus is a critical cause of atherosclerosis and in-stent restenosis [1,2]. Hyperglycemia caused aberrant vascular smooth muscle cells (VSMCs) proliferation and migration promote the occurrence of arterial neointimal hyperplasia which is an inevitable stage in the development of vascular remodeling [3–5]. Sustained hyperglycemia will shorten the diameter of blood vessels and vessel calcification hindering percutaneous coronary intervention efficacy [6,7]. Increasing evidence has demonstrated that inflammation, proliferation, advanced glycation end products, and oxidative stress caused by diabetes play a pivotal role in intimal hyperplasia, in which suppressing the abnormal proliferation and migration of VSMCs is reported as an effective method to restrain neointimal formation and vascular lumen loss in diabetes [8,9].

Poly (ADP-ribose) polymerase 1(PARP1) is a nuclear protein that performs DNA repair mainly by catalyzing its own poly ADP-ribosylation and other chromatin-related proteins [10]. In addition, PARP1 is also involved in a variety of cellular functions, including transcriptional regulation, cell cycle progression, cell migration, inflammation, and energy metabolism [11–13]. Reactive oxygen/-nitrogen species are effective activators of PARP1 due to the ability to damage DNA [14,15]. Recent studies have proven the increasing levels of oxidation in atherosclerotic plaques of DM mice, and carotid arteries after balloon injury in animal models [16–19]. However, to the best of our knowledge, no study has been reported regarding the role of PARP1 on neointimal hyperplasia caused by diabetes.

Tissue factor pathway inhibitor 2 (TFPI2) is a Kunitz-type serine

* Corresponding author. Qilu Hospital, Cheeloo College of Medicine, Shandong University, No.107, Wen Hua Xi Road, Jinan, Shandong, 250012, China.
** Corresponding author. Qilu Hospital, Cheeloo College of Medicine, Shandong University, No.107, Wen Hua Xi Road, Jinan, Shandong, 250012, China.
E-mail addresses: wzyclark56@126.com (Z.-y. Wang), shirlywy@126.com (Y. Wang), zhangmingxiang@sdu.edu.cn (M.-x. Zhang).
[1] These authors contributed equally.

https://doi.org/10.1016/j.redox.2021.102084
Received 29 June 2021; Received in revised form 26 July 2021; Accepted 26 July 2021
Available online 27 July 2021

proteinase repressor that is synthesized in large quantities of normal human tissue cells and secreted into the extracellular medium [20]. It has been reported that TFPI2 could inhibit plasmin and trypsin-mediated matrix metalloproteinase (MMP) activation [21], as well as directly inhibit the activity of MMPs [22–25]. Additionally, TFPI2 could suppress VSMCs proliferation by regulating cell cycle progression, which together with cell migration is an essential event in the process of neointimal formation [23,26]. Several studies have demonstrated that TFPI2 expression is largely diminished in atherosclerosis plaques, indicating that TFPI2 downregulation may contribute to neointimal hyperplasia and atherosclerosis progression [27,28]. Therefore, we speculated that PARP1 influences the process of neointimal hyperplasia dependent on TFPI2 expression under the condition of T1DM.

In the present study, we used human samples and T1DM murine models with a genetic deficiency in PARP1 to address the relationship between PARP1 and neointimal hyperplasia under the condition of diabetes. The result showed that hyperglycemia stimulated PARP1 abundance and genetic deficient in PARP1 attenuated the aorta remodeling process in STZ-treated mice. Furthermore, we proved the protective role of PARP1dificiency is dependent on the upregulation of TFPI2, which inhibits VSMCs proliferation and migration during the formation of neointima in diabetes mellitus.

2. Material and methods

2.1. Diabetic mouse model and carotid artery ligation

All experimental procedures were under the institutional animal care guidelines and approved by the Shandong University Animal Ethics Committee.

PARP1$^{+/-}$ mice were purchased as heterozygous breeding pairs from Jackson Laboratories (Bar Harbour, ME, USA). The wild type (PARP1$^{+/+}$) and PARP1 deficiency (PARP1$^{-/-}$) offspring were obtained from PARP1$^{+/-}$ mice were bred again. Mice were housed in a pathogen-free animal care facility at a constant temperature (24 °C) and a conventional light/dark cycle (12/12 h) under free conditions. The mice were randomized into the following three groups: (i) wild-type non-diabetic group (non-DM), (ii) wild-type diabetic group (DM), and (iii) PARP1−/− diabetic group (DM + PARP1−/−, n = 20, respectively). Type I diabetes was induced with 5 daily intraperitoneal injections of 50 mg/kg STZ in citrate buffer (0.05 mol/L; pH 4.5); control mice received an equivalent amount of citrate buffer solvents. Two weeks after the initial administration of STZ, mice with a blood glucose level of 16.7 mM (300 mg/dl) and above were considered diabetic and were included in the diabetic cohorts. Ligation of the left common carotid artery was performed just proximal to their bifurcations according to a procedure described previously 2 weeks after treatment with STZ or citrate solvent [29]. Mice were anesthetized. Postoperative analgesia was assured with 5 mg/kg SC carprofen. Animals were anesthetized at 3 weeks after surgery and sacrificed. Mice were fixed and perfused for 5 min with 4% formaldehyde in 0.1 mol/L sodium phosphate buffer (pH 7.3). The left and right carotid arteries were immersion-fixed in 70% ethanol. The length of common carotid arteries was 9 mm, of which the proximal and distal 2 mm were discarded and the remaining portion (5 mm) was cut in half. The two segments were embedded in paraffin, and serial sections (5 μm thick) were cut for analysis by immunostaining and hematoxylin-eosin staining for morphometry. Five or more sections spanning most of the vessel segment were analyzed for morphometry.

2.2. Human coronary artery samples

The human coronary arteries were obtained from both specimens with extensive diabetic atherosclerotic disease as well as healthy controls (n = 5). The human specimens were donated from the Shandong Red Cross Society (ethics approval No. KYLL-2018(KS)-233).

2.3. Histology and immunohistochemistry

Coronary artery morphologies were examined in 5 μm thick sections stained with hematoxylin. For immunohistochemical staining, paraffin-embedded tissue sections were dewaxed and stained with an antibody, followed by a biotin-conjugated secondary antibody (1:1000), and then with horseradish peroxidase-conjugated streptavidin (Dianova, Rodeo, CA). Histopathological features were analyzed using Image Pro-Plus 6.0 (Media Cybernetics, MD, USA). The area of positive staining for TFPI2 was expressed as the percentage of the stained area divided by the total intima area in at least 15 high amplification fields (400 ×). For immunofluorescence, the cells were first stained with specific antibodies and then staining with fluorescently labeled secondary antibodies. Nuclei were counterstained with 4′-6-diamidino-2-phenylindole (DAPI; Invitrogen). The images were analyzed by use of a LSM 710 laser confocal microscope (EC Plan-Neofluar 40x/1.30 Oil Objective) equipped with ZEN 2009 Light Edition software (Zeiss, Germany).

2.4. Cell culture and treatment

Human aortic smooth muscle cells (HASMCs, ATCC) were cultured in media containing apo-transferrin, fibroblast growth factor-2, insulin, insulin-like growth factor-1, hydrocortisone, and 5% fetal bovine serum. HASMCs (passages 4–6) were serum-deprived for 24 h to achieve synchronous growth, following which the cells were incubated in the medium with 5 mM D-glucose (normal control, NC), 5 mM D-glucose + 27.5 mM mannose (osmotic control, OC), 33 mM D-glucose (high glucose, HG), 33 mM D-glucose + 5 μM PARP1 inhibitor PJ34 (HG + PJ34), or 33 mM D-glucose + 5 μM DNMT-1 inhibitor 5-Aza-dC (HG+5-Aza-dC) for 72 h. Cells were grown at 37 °C in a 5% CO2 humidified incubator atmosphere.

2.5. Generation of TFPI2 expression constructs

The pcDNA3.1/V5-His TOPO Expression Kit (Invitrogen) was used to express TFPI2 (Invitrogen). The cDNA, containing the entire coding region was generated without a stop codon by RT-PCR and subcloned into pcDNA3.1/V5-His TOPO vector (pcDNA3.1/TFPI2) and pcDNA3.1/CT-green fluorescent protein (GFP), was used as a negative control for gene transfer into HASMCs.

2.6. Cell proliferation and cell cycle assay

Proliferation analysis was performed using the Cell-Light™ EDU assay kit (RiboBio, China), according to the manufacturer's instructions. The cells were collected 72 h after treatment, fixed with 20 °C with 70% ethanol, and then treated with ribonuclease (25 μg/mL) at 37 °C for 30 min, followed by staining with propidium iodide (PI, 50 μg/mL) in the dark at 4 °C for 30 min. The ratios of cells in G1, S, and G2/M phases were determined by FACS-Calibur flow cytometry (Becton Dickinson, USA).

2.7. Cell migration assay

HASMC migration assays were performed using transwell chambers (8-μm pore size; Corning Inc., Shanghai, China). Serum-starved HASMCs were seeded in the upper chamber, and the bottom chamber of the migration apparatus was filled with smooth muscle cell medium (SMCM) containing HG or OC. The cells were fixed with 4% formaldehyde and stained with crystal violet after culturing for 12 h. Cells were extracted on the surface with a cotton swab. Results are expressed as the average number of migrating cells per transwell membrane in 5 random fields of view (200 ×).

Table 1
Body weight and blood glucose measurements in mice 2 weeks after STZ injection.

Parameters	Non-DM	DM	DM + PARP1$^{-/-}$
Weight (g)	27.33 ± 1.91	23.61 ± 3.16*	23.08 ± 2.91*
Blood glucose (mM)	5.78 ± 0.66	23.8 ± 3.33*	23.1 ± 3.35*

The parameters were tested at 2 weeks after diabetes induction. 1. Body weight and blood glucose measurements. Non-DM: wild-type non-diabetic group; DM: wild-type diabetic group; DM + PARP1−/−: PARP1−/− diabetic group. All results are presented as the mean ± SEM. n = 20 per group. *p < 0.05 vs. non-DM.

2.8. Western blotting and gelatin zymography

Blots were incubated on a 10% polyacrylamide gel electrophoresis (SDS-PAGE) protein isolate, transferred to a polyvinylidene difluoride membrane, detected with PARP1 (Sigma, AV33754, Shanghai, China), PAR (Amy Jet, 4335-MC-100-AC, Wuhan, China), proliferating cell nuclear antigen (PCNA; Abcam, ab29, Shanghai, China), MMP2 (Abcam, ab37150), MMP9 (Abcam, ab38898), TFPI2 (Abcam, ab186747), and β-actin (2SGB-BIO, TA-09, Shanghai, China) overnight at 4 °C, and developed with chemiluminescence. MMP activity assay was performed using gelatin zymography. The cell culture supernatants were electrophoresed in a 10% polyacrylamide gel containing 1 mg/mL gelatin. The gelatin dissolution band represented active MMP2 and MMP9.

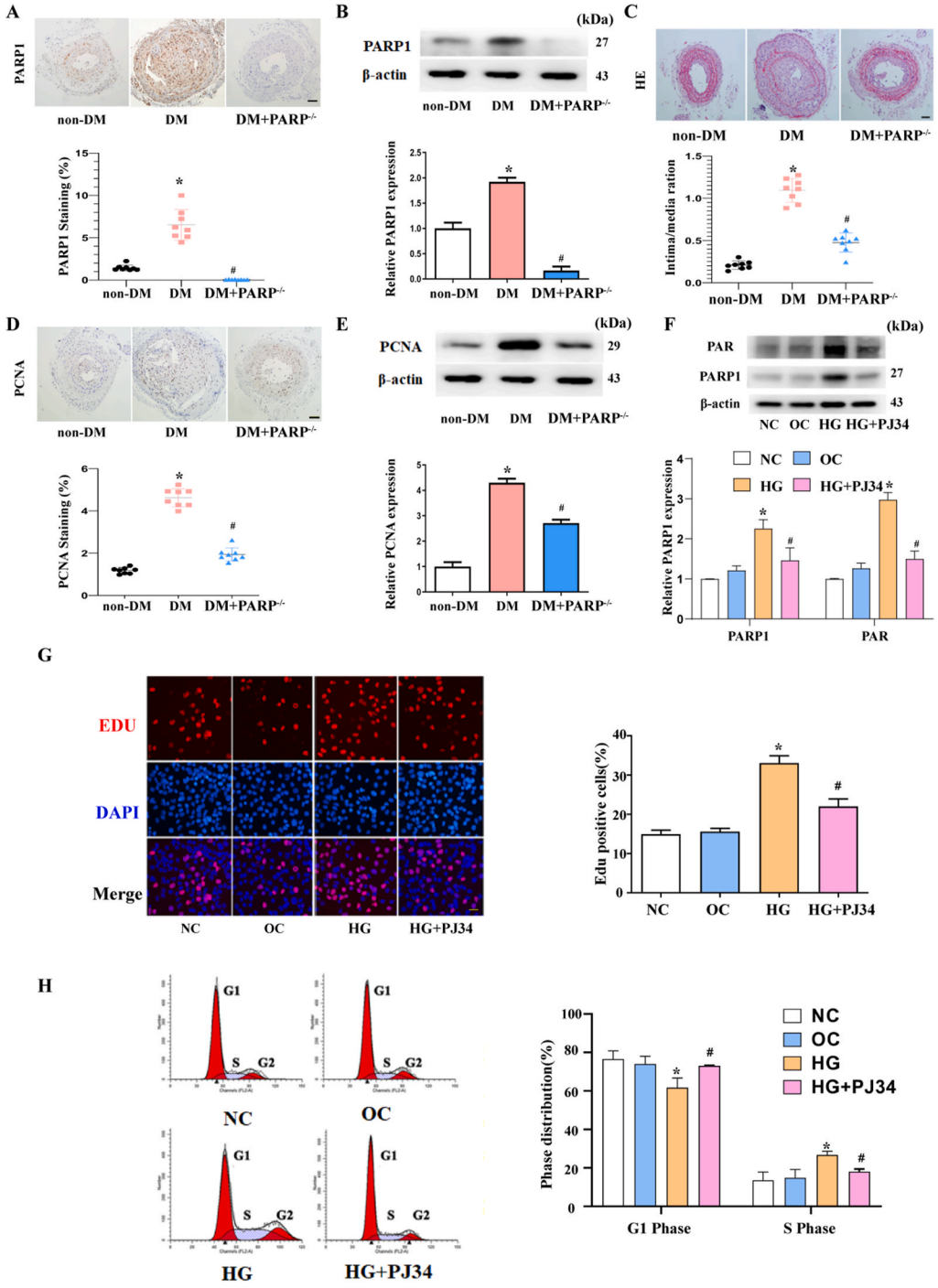

Fig. 1. PARP1 Participates in Cell Proliferation and Neointimal Formation in Diabetes. (A) Immunohistochemical staining and quantification of PARP1 in the neointima of the carotid artery of mice (scale bar: 50 μm, N = 8 in each group). Non-DM, wild type non-diabetic group; DM, wild-type diabetic group; DM + PARP1−/−, PARP1−/− diabetic group. *p < 0.05 vs. non-DM; #p < 0.05 vs. DM. (B)Western blotting of PARP1 protein expression in the ligated carotid arteries of mice (N = 5 in each group). *p < 0.05 vs. non-DM; #p < 0.05 vs. DM. (C) Hematoxylin and eosin (HE) staining of the carotid artery of mice and quantification analysis of intima/media ratio (scale bar: 50 μm, N = 8 in each group). *p < 0.05 vs. non-DM; #p < 0.05 vs. DM. (D) Immunohistochemical staining and quantification of PCNA in the neointima of the carotid artery of mice (scale bar: 50 μm, N = 8 in each group). *p < 0.05 vs. non-DM; #p < 0.05 vs. DM. (E) Western blotting of PCNA protein expression in the ligated carotid arteries of mice (N = 5 in each group). *p < 0.05 vs. non-DM; #p < 0.05 vs. DM. (F) Western blot analysis of PARP1 protein expression in HASMCs. NC, negative control (5.5 mM D-glucose); OC, osmotic control (5.5 mM D-glucose + 27.5 mM mannose); HG, high glucose (33 mM D-glucose); HG + PJ34, high glucose (33 mM D-glucose) + 5 μM PJ34. The values shown represent the mean ± SEM of independent assays. N = 5 per group, *p < 0.05 vs. OC; #p < 0.05 vs. HG. (G) Immunofluorescence of EDU staining. Nuclei were counterstained with DAPI (blue); red staining indicates cells undergoing proliferation. The EDU-positive index was expressed as a percentage (positive/total cell number). Scale bar: 10 μm. N = 4 per group, *p < 0.05 vs. OC; #p < 0.05 vs. HG. (H) Flow cytometry of the cell cycle. The relative percentage of cells in different cell cycle phases was reported, whereas the percentage of apoptotic events was ignored. N = 4 per group, *p < 0.05 vs. OC; #p < 0.05 vs. HG. (For interpretation of the references to color in this figure legend, the reader is referred to the Web version of this article.)

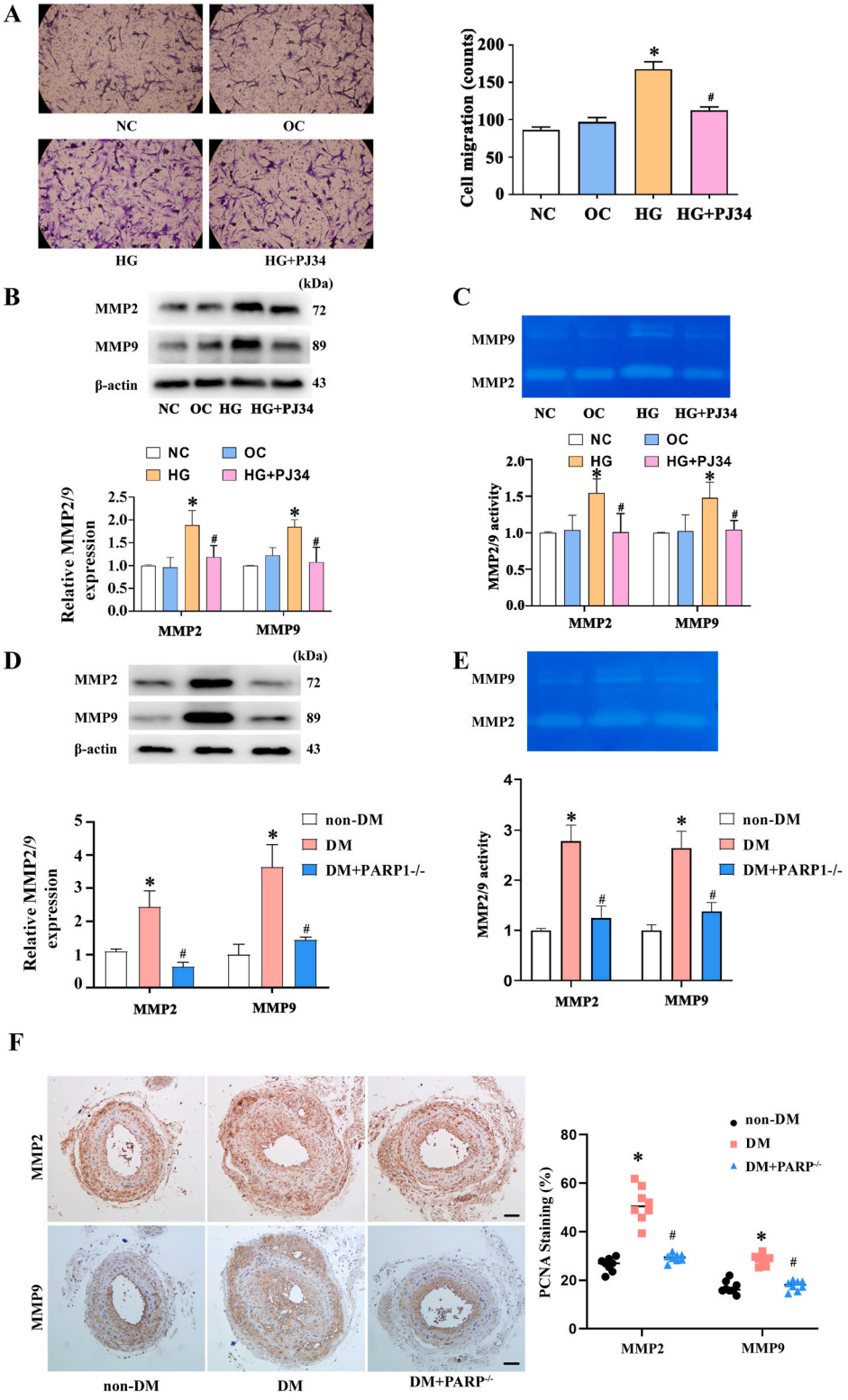

Fig. 2. PARP1 Participates in Cell Migration in Diabetic Neointimal Formation. (A) Transwell migration assay: The percentage of migrated cells relative to the control was quantified (scale bar: 20 μm). N = 4 in each group, *p < 0.05 vs. OC; #p < 0.05 vs. HG. (B) Western blotting of MMP2 and MMP9 protein expression in HASMCs after 72 h of high glucose stimulation. NC, negative control; OC, osmotic control; HG, high glucose; HG + PJ34, high glucose + PJ34. N = 5 per group,*p < 0.05 vs. OC; #p < 0.05 vs. HG. (C) Gelatin zymography of MMP2 and MMP9 activities in HASMCs after 72 h of high glucose stimulation. N = 5 per group, *p < 0.05 vs. OC; #p < 0.05 vs. HG. (D) and (E) Western blotting and Gelatin zymography analysis of MMP2 and MMP9 in the neointima of the carotid artery of mice. Non-DM, wild type non-diabetic group; DM, wild-type diabetic group; DM + PARP1−/−, PARP1−/− diabetic group. N = 5 in each group, *p < 0.05 vs. non-DM;; #p < 0.05 vs. DM. (F) Immunohistochemical staining and quantification of MMP2 and MMP9 in the neointima of the carotid artery of mice (scale bar: 50 μm, N = 8 in each group). *p < 0.05 vs. non-DM; #p < 0.05 vs. DM.

2.9. Microarray analysis

The microarray data in this publication have been deposited in the National Center for Biotechnology Information's Gene Expression Omnibus (GEO; https://www.ncbi.nlm.nih.gov/geo/index.cgi; GSE141193).

HASMCs were treated with PARP1 inhibitor PJ34 or PBS, using RNeasy Mini Kit (Qiagen, Hilden, Germany) purified total RNA. Concentration and purity were detected using a NanoDrop-1000 Spectrophotometer (Thermo Fisher Scientific) and an Agilent 2100 Bioanalyzer (Agilent Technologies, Santa Clara, CA, USA). Biotin-labeled cRNA was synthesized using the GeneChip 3 IVT PLUS Reagent Kit (Thermo Fisher Scientific). Each sample was hybridized to a GeneChip™ Human Transcriptome 2.0 Array (Thermo Fisher Scientific) after fragmentation.

The procedure was carried out according to the manufacturer's

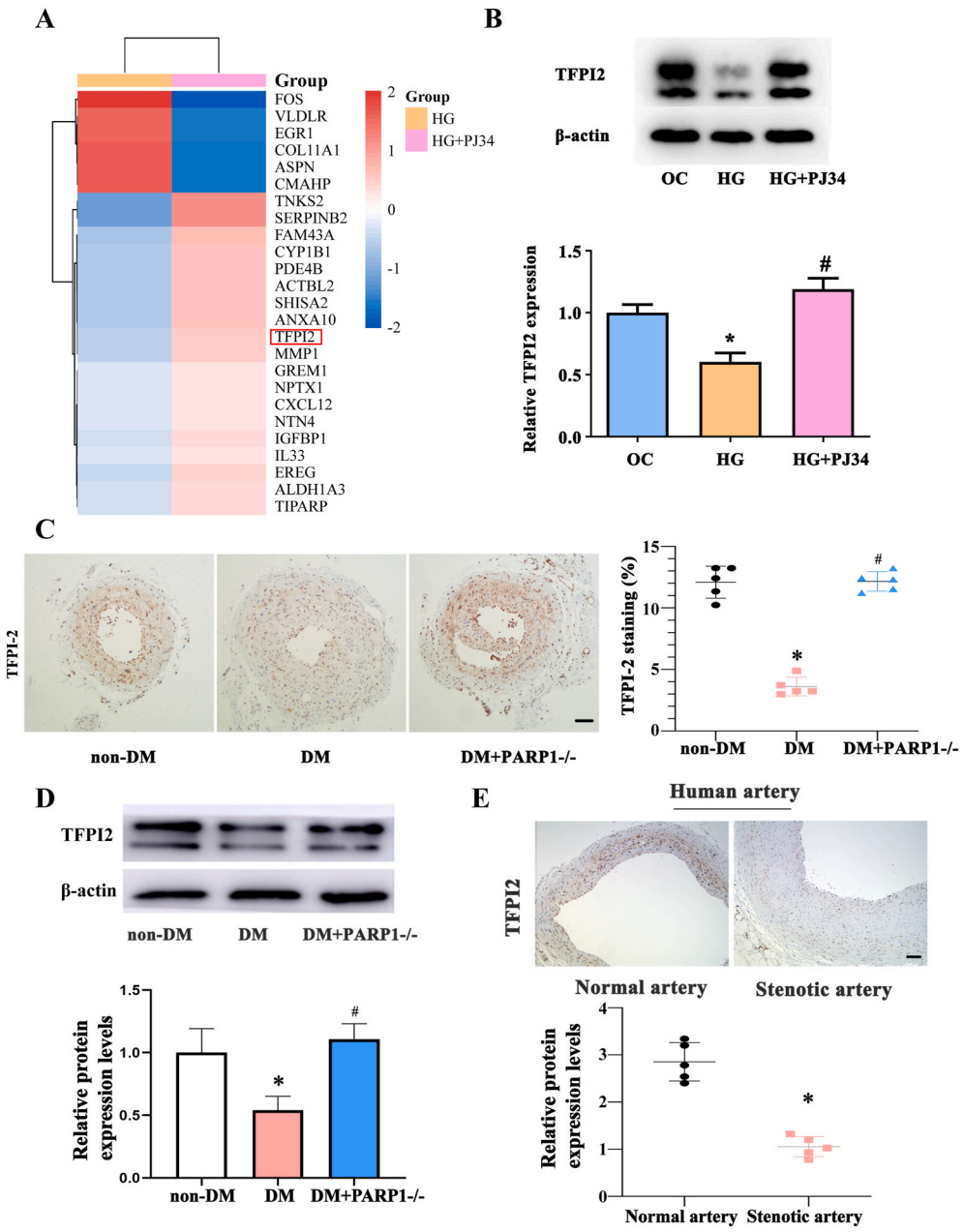

Fig. 3. PARP1 Inhibition Attenuates Diabetic Neointimal Formation by Targeting TFPI2. (A) Heatmap showing the expression profile of DEGs with >2.5-fold upregulation or ≥ 1.5-fold downregulation in high glucose-stimulated HASMCs with PARP1 inhibition. HG, high glucose; HG + PJ34, high glucose + PJ34 (B) Western blotting of TFPI2 protein expression in HASMCs with and without PARP1 inhibition. N = 3 per group, *P < 0.05 vs. OC; #p < 0.05 vs. HG. (C) Immunohistochemical staining of TFPI2 in the neointima of the carotid artery of mice (scale bar: 50 μm). N = 5 per group, *p < 0.05 vs. non-DM; #p < 0.05 vs. DM. (D) Western blotting of TFPI2 protein expression in the neointima of the carotid artery of mice. N = 5 in each group, *p < 0.05 vs. non-DM; #p < 0.05 vs. DM. (E) Immunohistochemical staining of TFPI2 in the neointima of the human coronary artery and quantification (scale bar: 100 μm). N = 5 per group,*p < 0.05 vs. normal artery.

protocol. The statistical software R (ver. 2.7.2, 3.1.2) was used for statistical analysis. The CEL files were normalized using the DFW method (R ver. 2.7.2), and PCA analysis was conducted using R ver. 3.1.2. The Rank Product method using R ver. 3.1.2) was employed and standard probe that met the false discovery rate (FDR < 0.05) criterion were extracted as differentially expressed genes (DEGs). Canonical pathway analysis of the DEGs was performed using Qiagen's Ingenuity Pathway Analysis (IPA, www.qiagen.com/ingenuity). (Qiagen).

Pathways with p-values < 0.05 and | z-scores | 2 were considered significant modulations.

2.10. Detection promoter DNA hypermethylation of TFPI2

Genomic DNA (1 g) purified from HASMCs using a QIAamp DNA Minikit (Qiagen, Valencia, CA) was modified with sodium bisulfate using the EZ DNA methylation toolkit (Zymo Research, Orange, CA). The MassARRAY platform (Sequenom, San Diego, CA) was used to determine DNA methylation levels as described previously [30]. The detailed primers were designed using the online software Epidesigner (at http://www.epidesigner.com/). For each reverse primer, an additional T7 promoter tag was added for in vivo transcription, while a 10-m tag was used on the forward primer to adjust the melting temperature difference. The following primers based on the reverse complementary strands of the TFPI2-promoter were used:

(5′-AGGAAGAGAGGGAATTTATTTTTGAAGGTATGAA-3′ and 3′-CAGTAATACGACTACCTATAGGGAGAAGGCTCCTCCCAAAA-TACTAAAATTACAAA-5′). Analysis of methylation data for individual units (1–3 CpG sites per unit) using EpiTyper software (Sequenom).

2.11. Statistical analysis

SPSS statistical software (SPSS Inc., Chicago, IL) and GraphPad Prism 8 (GraphPad Software) were used for statistical analyses. Parameters such as size of the samples, number of independent experiments (mean ± SD), and statistical significance are illustrated in the figures and figure legends. After verification of the normal distribution of the data,

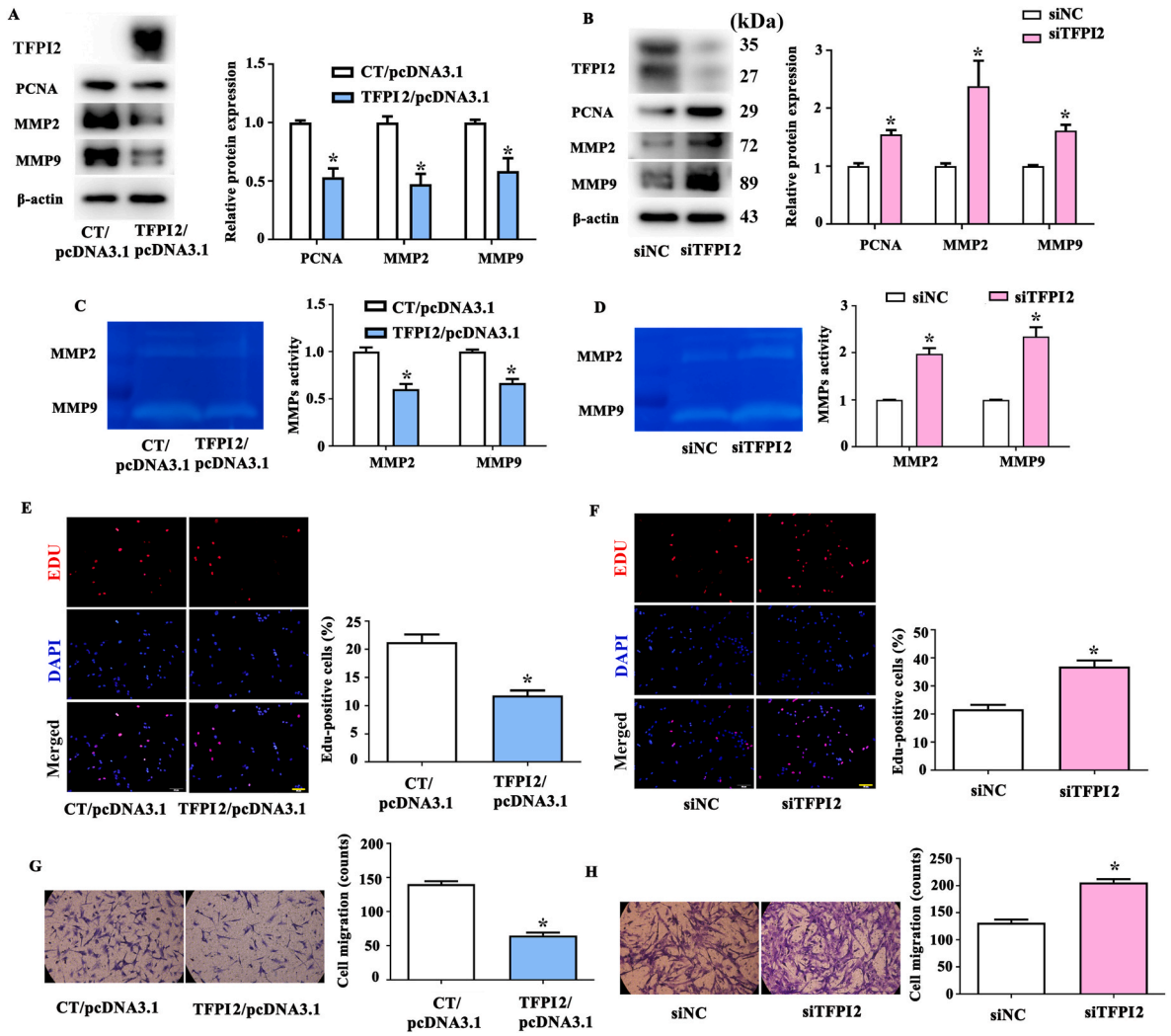

Fig. 4. Effects of TFPI2 on HASMC Proliferation and Migration. (A) and (B) Western blotting of PCNA, MMP2, and MMP9 protein expression with TFPI2/pCDNA3.1 or siTFPI2 transfection in HASMCs. N = 3 per group. (C) and (D) Gelatin zymography of MMP2 and MMP9 activity with TFPI2/pCDNA3.1 or siTFPI2 transfection in HASMCs. N = 3 in each group. (E) and (F) EDU staining of HASMCs with TFPI2/pCDNA3.1 or siTFPI2 transfection. Scale bar: 100 μm. N = 3 per group. (G) and (H) Transwell migration assays of HASMCs with TFPI2/pCDNA3.1 or siTFPI2 transfection. *p < 0.05 vs. control group. N = 3 per group.

statistical differences were evaluated with Student *t*-test for two groups and one-way ANOVA for three or more groups (Tukey's post-test). P < 0.05 was considered statistically significant.

3. Results

3.1. PARP1 deficiency protects against hyperglycemia-induced augmented neointimal hyperplasia by inhibition of HASMC proliferation

To prove the involvement of PARP1 in hyperglycemia augmented neointimal hyperplasia, we firstly used STZ injection to induce DM, where the blood glucose levels of DM group increased to >23 mM versus 5.78 mM in control group (Table 1; n = 20; P < 0.05). Carotid arteries were ligated 2 weeks after STZ or citrate treatment and collected for analysis 3 weeks after surgery. Using immunochemical and western-blot analysis, we found the expression of PARP1 elevated apparently in DM group (Fig. 1A and B). Meanwhile, PARP1−/− diabetic mice displayed dramatically decreased neointimal thickening compared to the wildtype group (Fig. 1C). According to immunochemical staining and Western-blot, we analyze the proliferation of neointimal VSMCs using PCNA (proliferating cell nuclear antigen), an indicator of cell proliferation. An elevated PCNA protein level was seen in diabetic mice while decreased PCNA protein expression in PARP1 deficient diabetic mice (Fig. 1D and E).

To further determine the role that PARP1 plays in regulating HG-induced VSMCs proliferation, 5 μM PJ34 treatment was used to inhibit PARP1 expression. HG treatment significantly increased the PARP1 and PAR (an enzymatic product of PARP1) by approximately two times, while PJ34 treatment reduced its protein level (p < 0.05, Fig. 1F). Moreover, cell proliferation was demonstrated using the EDU incorporation assay. Compared with the control group, HG increased EDU incorporation, and PJ34 treatment reversed the increase in EDU incorporation (Fig. 1G). In order to explore the potential mechanism of PARP1 inhibition in the proliferation of VSMCs, we performed cell cycle analysis on high glucose-stimulated VSMCs by measuring the DNA content of cells stained with sodium iodide. There was a decline in cells corresponding to the G1 phase and an increase in cells corresponding to the S phase in the high glucose-stimulated VSMCs compared with the control, and PARP1 inhibition reduced the high glucose mediated transition from the G1 to the S phase in VSMCs (Fig. 1H).

3.2. PARP1 deficiency inhibits glycemia-induced VSMCs migration and attenuates the enzymatic activity and expression of MMPs

To better illustrate the effect of PARP1 on glycemia-induced VSMCs Migration, we used the transwell migration test finding that genetic

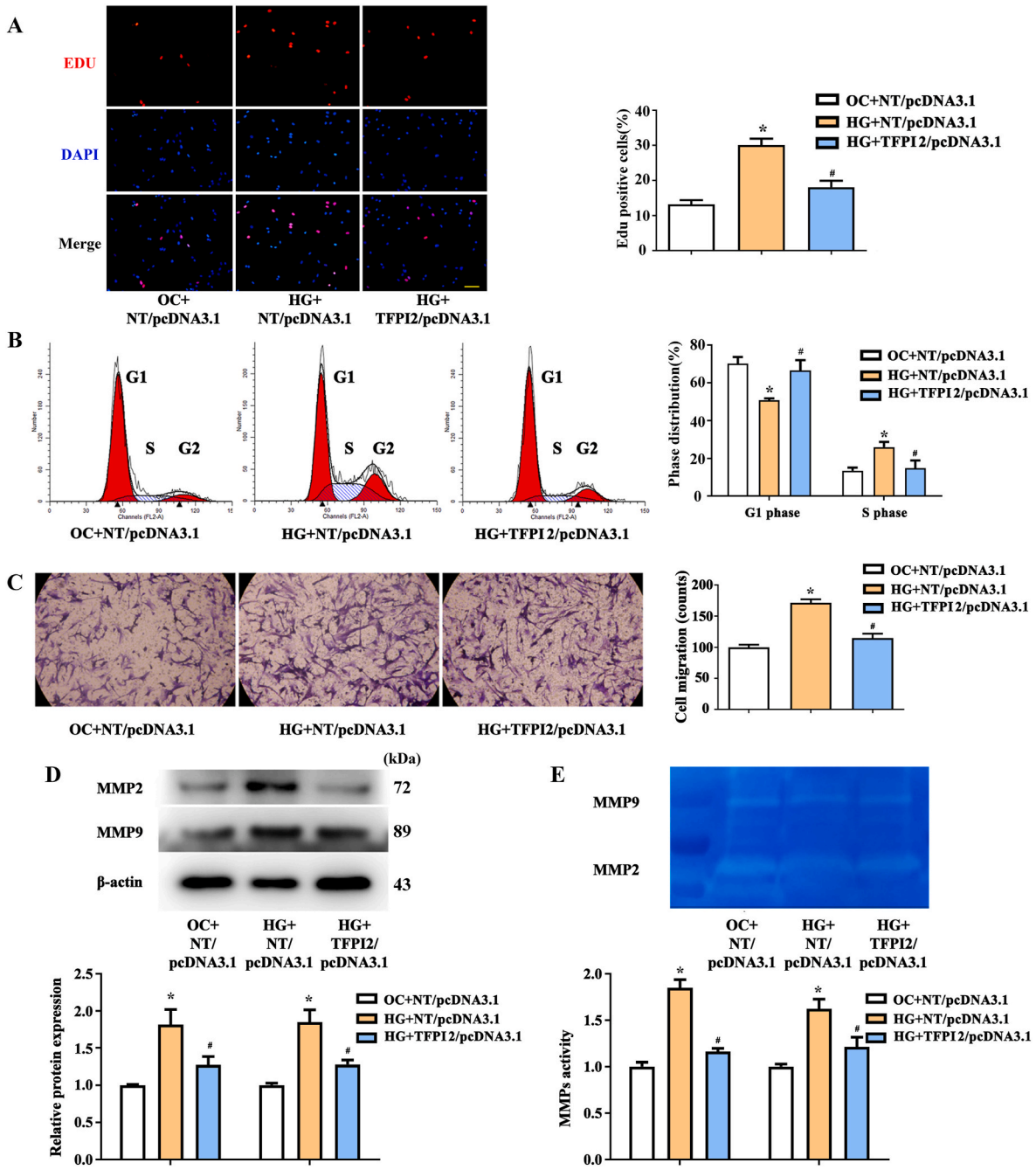

Fig. 5. Effects of TFPI2 on the Proliferation and Migration of High Glucose-stimulated HASMCs. (A) EDU staining of high-glucose stimulated HASMCs with TFPI2/pCDNA3.1 transfection (Scale bar: 100 μm). *P < 0.05 vs. OC + NT/pcDNA3.1; #p < 0.05 vs. HG + NT/pcDNA3.1. N = 3 per group. (B) Flow cytometry of the cell cycle. N = 3 in each group, *P < 0.05 vs. OC + NT/pcDNA3.1; #p < 0.05 vs. HG + NT/pcDNA3.1. (C) Transwell migration assays of high-glucose-stimulated HASMCs with TFPI2/pCDNA3.1 transfection. N = 3 in each group,*P < 0.05 vs. OC + NT/pcDNA3.1; #p < 0.05 vs. HG + NT/pcDNA3.1. (D) Western blotting of MMP2 and MMP9 protein expression. (E) Gelatin zymography of MMP2 and MMP9 activities. N = 3 in each group,*P < 0.05 vs. OC + NT/pcDNA3.1; #p < 0.05 vs. HG + NT/pcDNA3.1.

inhibition of PARP1 significantly suppressed high glucose-stimulated cell migration (Fig. 2A). Moreover, we observed that PJ34 treatment markedly attenuated the high glucose-induced increase in MMP2 and MMP9 protein expression, consistent with the changes in gelatin zymography of MMP activity (Fig. 2B and C). Furthermore, the immunostaining and gelatin zymography analysis revealed that the expression and activity levels of MMP2 and MMP9 were significantly increased in the neointima of diabetic mice compared with the controls, whereas PARP1 deletion markedly decreased their intensity (Fig. 2D and E). Meanwhile, consistent results were found using immunochemical analysis (Fig. 2F).

3.3. PARP1 downregulates TFPI2 gene expression

Genome microarray assays of HASMCs with or without PARP1 inhibition were performed to profile DEGs that might be involved in PARP1 regulation. A heat map was used to illustrate the expression profile of DEGs (>2-fold) in untreated and PJ34-treated HASMCs (Fig. 3A). Among these genes, TFPI2 was the one exhibiting the greater down-regulation change in expression (>3.65-fold). Some studies have

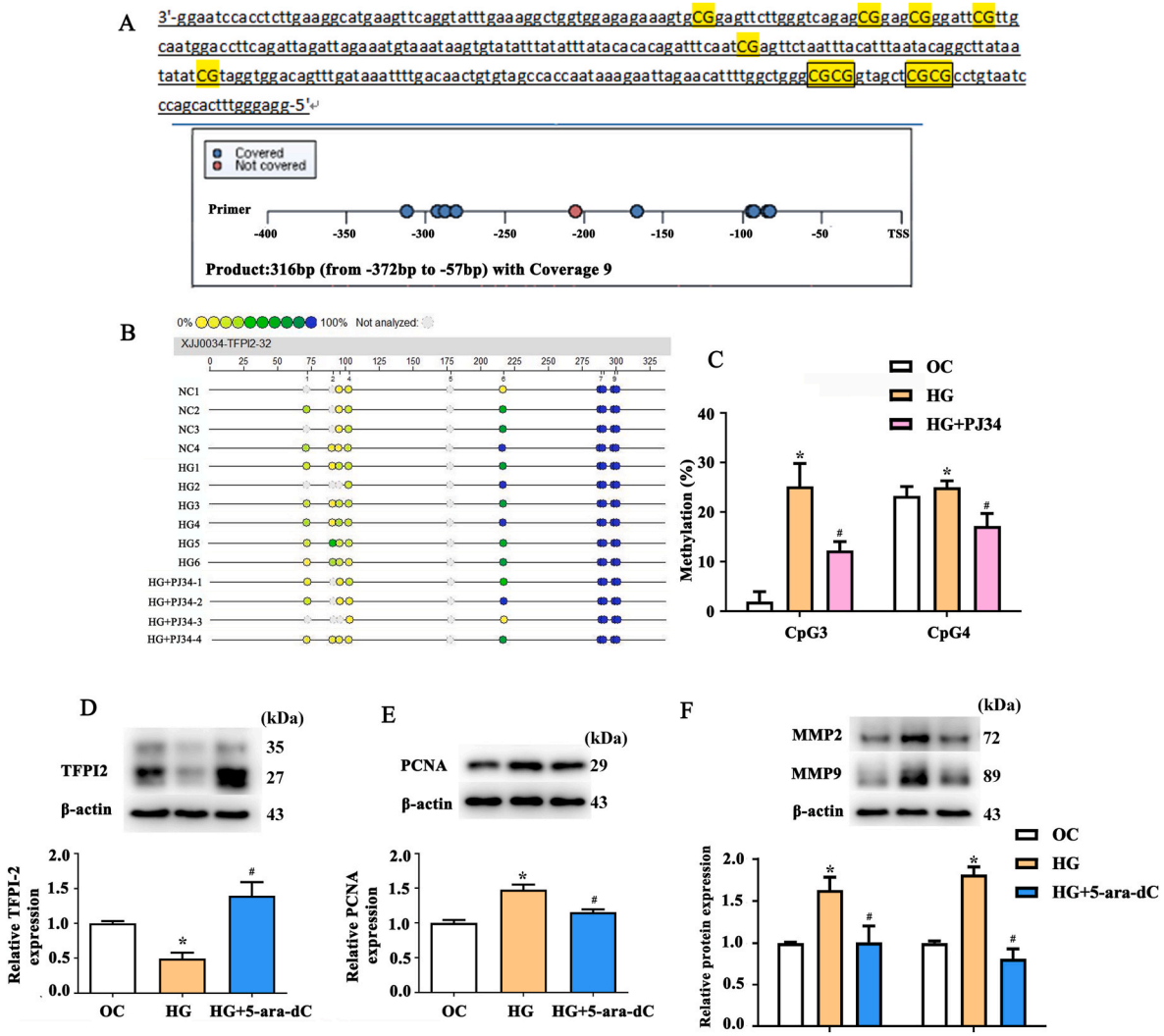

Fig. 6. PARP1 Mediated High Glucose-induced CpG Island Methylation in TFPI2 Promoter. (A) The CpG islands in the promoter of the TFPI2 region immediately upstream −372 bp to −57 bp, which are relative to the translation start sites, were analyzed, wherein a total of 10 CpG islands were divided into 8 CpG units (yellow highlight). (B) Quantitative CpG island methylation analysis: The colors of each circle represent the CpG island methylation level of each corresponding CpG unit. Yellow (~0% methylation), green (~50% methylation), and dark blue (~100% methylation). The white circles represent the missing data at a given CpG site. (C) Quantitative CpG island methylation analysis at CpG_3 and CpG_4 sites. The quantitative data represent the results of three independent experiments. (D), (E) and (F) Western blotting of the TFPI2, PCNA, MMP2, and MMP9 proteins in HASMCs treated with or without the 5-aza-dC methyltransferase inhibitor. 5-aza-dC seemed to recover the high glucose-stimulated TFPI2 depression in HASMCs. N = 3 in each group, *P < 0.05 vs. OC; #p < 0.05 vs. HG. (For interpretation of the references to color in this figure legend, the reader is referred to the Web version of this article.)

reported that TFPI2 closely corresponds to the process of VSMCs proliferation and migration by regulating MMP2 and MMP9 [22–24] , so we chose TFPI2 as a target regulated by PARP1 in the present study. To verify the microarray analysis data, we examined TFPI2 expression by western blotting. What's more, PJ34 treatment evidently reversed the reduced TFPI2 expression due to high glucose (Fig. 3B). Immuno-analysis also showed that TFPI2 levels in the neointima of the carotid artery and tunica media of the aorta were markedly lower in diabetic mice than in control mice, which were reversed in PARP1−/− diabetic mice (Fig. 3C and D). In addition, lower TFPI2 expression was observed in the neointima of stenotic coronary arteries of diabetic patients than in that of healthy controls (Fig. 3E).

3.4. TFPI2 mediates HASMC proliferation and migration

Furthermore, we evaluated the role of TFPI2 in the proliferation and migration of HASMCs. HASMCs cultured in DMEM were transfected with pcDNA3.1/TFPI2 or siRNA for TFPI2.

TFPI2 overexpression significantly inhibited PCNA, MMP2, and MMP9 expression (Fig. 4A). Further validation by TFPI2 knockdown showed increased expression of PCNA, MMP2, and MMP9 protein (Fig. 4B). The gelatin zymography of MMP2 and MMP9 activity showed results that were consistent with the above conclusions (Fig. 4C and D). TFPI2 overexpression was associated with decreased EDU incorporation, and the TFPI2 knockdown obviously increased the incorporation as compared with siNC transfected cells (Fig. 4E and F). Additionally, overexpressed TFPI2 led to waning migration of HASMCs, whereas TFPI2 silencing promoted the migration than the siNC control (Fig. 4G and H).

3.5. TFPI2 overexpression inhibits HG-induced HASMC proliferation and migration

We then investigated the mechanism of TFPI2 expression on neointimal formation in diabetes. The pcDNA3.1/TFPI2 transfected into HASMCs can significantly inhibit the proliferation of hyperglycemia-

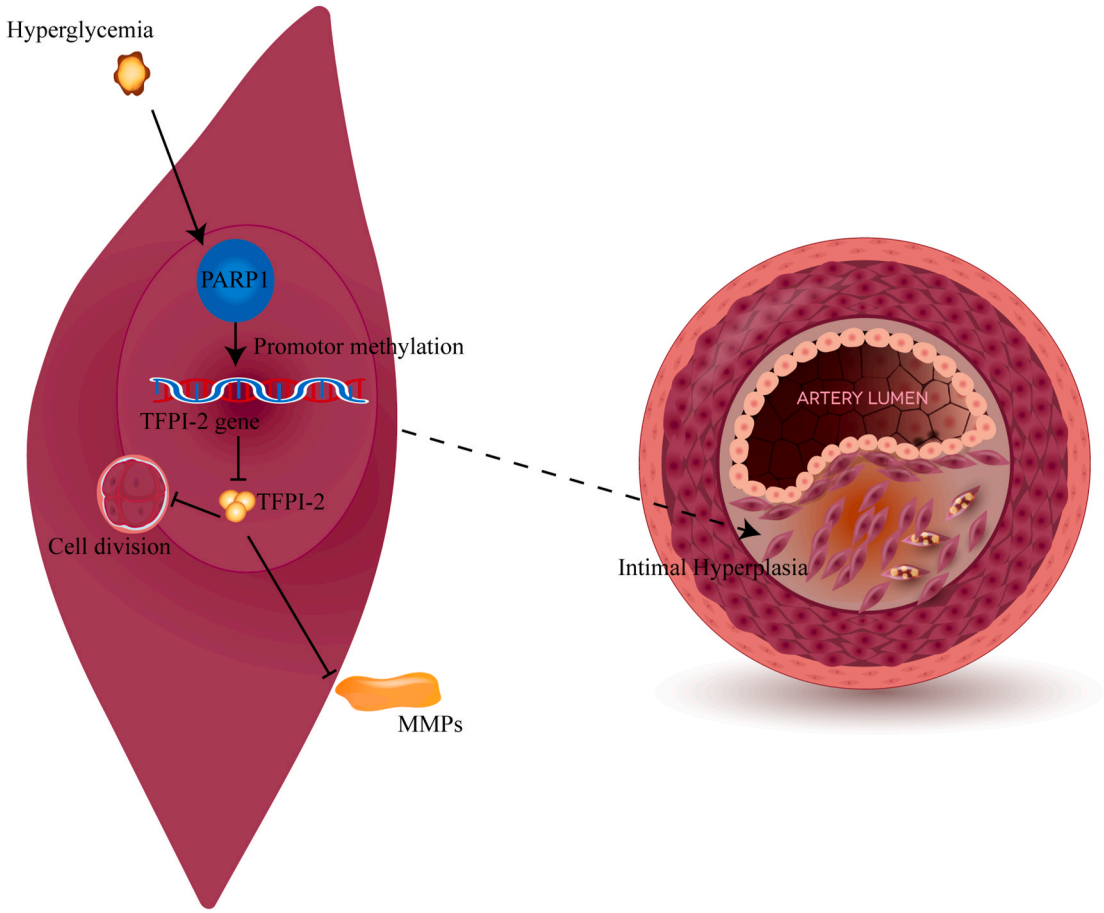

Fig. 7. Model of PARP1 Dependent Regulation Of TFPI2 Activity Enhancing Hyperglycemic-induced Neointimal Hyperplasia. DNA damage caused by hyperglycemia leads to PARP1 activity augmentation in VSMCs. Loss of PARP1 results in elevated TFPI2 gene expression through DNA hypomethylation. Activation of TFPI2 leads to decreased VSMCs proliferation and migration and suppressed excessive intimal hyperplasia in diabetes.

induced HASMCs compared with negative control (pcDNA3.1/CT-green; Fig. 5A). Flow cytometry showed that increased G1 phase and decreased S phase were found in high-glucose-stimulated HASMCs compared to the controls, while TFPI2 overexpression reduced high glucose-mediated transition from G1 to S phase in HASMCs (Fig. 5B). Transwell migration assays revealed that TFPI2 overexpression reduced the high glucose-stimulated HASMC migration (Fig. 5C). Moreover, TFPI2 overexpression markedly attenuated the high glucose-induced increase in MMP2 and MMP9 protein expression, which is consistent with the changes in the gelatin zymography of MMP activity (Fig. 5D and E).

3.6. PARP1 mediated HG-induced TFPI2 promoter DNA methylation

Studies have shown that the TFPI2 promoter contains some of the CpG islands participating in transcriptional silencing [31–33]. To determine whether PARP1 mediates hyperglycemia-induced TFPI2 promoter DNA methylation thus decreasing TFPI2 activity, the methylation levels of CpG islands in the TFPI2 promoter were examined using the MassARRAY assay (Sequenom).

One region in the TFPI2 promoter (−372 bp to −57 bp, nucleotide positions relative to the translation initiation sites) was analyzed, wherein all 10 CpG sites were divided into 8 CpG units (Fig. 6A). We found that the methylation status at the CpG_3 site was much higher in the high-glucose-stimulated HASMCs than in the control groups, whereas PARP1 inhibition significantly decreased the high glucose-stimulated methylation levels at the CpG_3 and CpG_4 sites (Fig. 6B and C). To assess whether hyperglycemia-induced DNA methylation was responsible for TFPI2 suppression, we treated HAECs transfected with 5-M 5-ara-dC, a methyltransferase inhibitor, for 36 h. TFPI2 suppression was reversed by 5-ara-dC treatment as shown by western blotting (Fig. 6D). Meanwhile, 5-ara-dc also significantly reduced the expression of PCNA and MMP2/MMP9 in HASMCs induced by hyperglycemia (Fig. 6E and F).

4. Discussion

PARP1, a nuclear protein participating in DNA repair, showed an elevated expression in diabetes due to increased DNA damage caused by hyperglycemia [16,17]. PARP-1 activation plays a key role in the pathogenesis of various diabetic complications such as vasculopathy, cardiomyopathy, retinopathy and neuropathy [8,34]. However, its specific role in neointimal hyperplasia in diabetes and precise molecular mechanisms have not been clarified. Here, we confirmed a higher PARP1 abundance in the pathogenesis of neointimal hyperplasia in both humans and mice. Recently, emerging evidence shows that PARP1 is involved in various cellular processes, such as inflammatory response, vascular function, cell proliferation and migration, independent of its classic function of DNA repair [10–13,35–37]. A previous study showed that minocycline suppressed VSMCs proliferation and plaque formation by inhibiting PARP1 and inducing CDK inhibitor p27 expression [38]. It has also been reported that PARP1 inhibition could promote the trans-migration of VSMCs to the intima of atherosclerotic plaques by increasing metalloproteinase 2, a tissue inhibitor, and thus enhancing the plaque stability [18]. Using PARP1 knockdown mice, our study is the first to prove that genetic inhibition of PARP1 significantly alleviated

neointimal thickening in diabetic mice by inhibiting glucose-stimulated VSMCs proliferation dependent on the G1-S phase transition, as well as impeding VSMCs migration by suppressing MMP2/9 expression and activity in vitro and vivo.

TFPI-2, as a Kunitz-type serine proteinase inhibitor, is mainly synthesized by VSMCs and endothelial cells [39]. It has been reported that TFPI2 is expressed in a variety of human tissue cells such as the heart, skeletal, muscle, liver, pancreas, and kidney tissues, wherein the protein is secreted into the extracellular matrix (ECM) and prevents ECM hydrolysis by inhibiting the activation of plasmin-mediated MMPs [24,40]. In addition, TFPI2 has been discovered to be widely distributed in the cytoplasm and nucleus. Interaction of the nuclear-localized TFPI2 with a transcription factor AP-2α results in inhibition of cell migration by negatively regulating the transcription of MMP2 mRNA in breast cancer cells [41]. Moreover, as a direct inhibitor of MMP-2 and MMP-9 and potent inhibitor of both matrix-bound and cell-associated plasmin, TFPI-2 was reported to inhibit the progression of atherosclerosis and promote atherosclerotic plaque stability [42,43]. Our study found TFPI2 overexpressed under the condition of PARP1 inhibition using transcriptome analysis, and TFPI2 could efficiently inhibit the hyperglycemia-induced VSMCs proliferation and migration.

DNA methylation, a biological process where methyl groups are added to the DNA molecule, typically represses gene transcription via inhibiting the binding of transcription factor(s) to DNA [44]. PARP1 has been reported to play an important role in gene regulatory pathways including basal transcription machinery, histone modifications, chromatin remodeling, and DNA methylation [11]. Moreover, promoter region analysis of TFPI-2 gene 5′-flanking region revealed a high GC-rich content with masses of CpG sites. Transcription of TFPI2 is often silenced by aberrant promoter hypermethylation in tumor tissues [45].Furthermore, it has also been demonstrated that TFPI2 promoter methylation is linked to low activity in carotid atherosclerotic plaques [28]. In this article, we used the MassARRAY platform validating that high glucose-stimulated PARP1 upregulation promoted TFPI2 hypermethylation, which also accounts for its low expression in vascular neointima.

In conclusion, PARP1 overexpression in diabetes caused excessive VSMC proliferation, migration, and intimal hyperplasia via silencing TFPI2 through DNA hypermethylation (Fig. 7). Understanding this pathway provides important molecular insights into PARP1 for diabetic neointimal hyperplasia treatment. Further studies are needed to elucidate the underlying mechanism by which PARP1 regulates downstream molecules.

Funding

This work was supported by the National Natural Science Foundation of China (#81100206, #82000417 and #81970251), the Taishan Scholar Project of Shandong Province of China (No. ts20190972), 2020SFXGFY06 and Key Issues of Jinan Science and Technology Bureau (#20170409).

Declaration of competing interest

None.

References

[1] J. Yang, P. Zeng, J. Yang, X. Liu, J. Ding, H. Wang, et al., MicroRNA-24 regulates vascular remodeling via inhibiting PDGF-BB pathway in diabetic rat model, Gene 659 (2018) 67–76, https://doi.org/10.1016/j.gene.2018.03.056. PubMed PMID: 29559348.

[2] J. Xu, L. Li, H.F. Yun, Y.S. Han, MiR-138 promotes smooth muscle cells proliferation and migration in db/db mice through down-regulation of SIRT1, Biochem. Biophys. Res. Commun. 463 (4) (2015) 1159–1164, https://doi.org/10.1016/j.bbrc.2015.06.076. PubMed PMID: 26079878.

[3] D. Kruger, Neo-intimal hyperplasia, diabetes and endovascular injury, Cardiovasc. J. Africa 23 (9) (2012) 507–511, https://doi.org/10.5830/CVJA-2012-019. PubMed PMID: 22618688; PubMed Central PMCID: PMC3721904.

[4] R.N. Mitchell, P. Libby, Vascular remodeling in transplant vasculopathy, Circ. Res. 100 (7) (2007) 967–978, https://doi.org/10.1161/01.RES.0000261982.76892.09. PubMed PMID: 17431198.

[5] U. Kansakar, S.S. Jankauskas, J. Gambardella, G. Santulli, Targeting the phenotypic switch of vascular smooth muscle cells to tackle atherosclerosis, Epub 2021/04/10, Atherosclerosis 324 (2021) 117–120, https://doi.org/10.1016/j.atherosclerosis.2021.03.034. PubMed PMID: 33832772; PubMed Central PMCID: PMCPMC8195811.

[6] M. Son, S. Oh, J.T. Jang, C.H. Park, K.H. Son, K. Byun, Attenuating effects of pyrogallol-phloroglucinol-6,6-bieckol on vascular smooth muscle cell phenotype changes to osteoblastic cells and vascular calcification induced by high fat diet, Epub 2020/09/17, Nutrients 12 (9) (2020), https://doi.org/10.3390/nu12092777. PubMed PMID: 32932908; PubMed Central PMCID: PMCPMC7551448.

[7] X.J. Sun, W.Q. Ma, Y. Zhu, N.F. Liu, POSTN promotes diabetic vascular calcification by interfering with autophagic flux, Epub 2021/03/22, Cell. Signal. 83 (2021) 109983, https://doi.org/10.1016/j.cellsig.2021.109983. PubMed PMID: 33744420.

[8] T.V. Fiorentino, A. Prioletta, P. Zuo, F. Folli, Hyperglycemia-induced oxidative stress and its role in diabetes mellitus related cardiovascular diseases, Curr. Pharmaceut. Des. 19 (32) (2013) 5695–5703. PubMed PMID: 23448484.

[9] Y. Wang, W.Q. Ma, Y. Zhu, X.Q. Han, N. Liu, Exosomes derived from mesenchymal stromal cells pretreated with advanced glycation end product-bovine serum albumin inhibit calcification of vascular smooth muscle cells, Epub 2018/10/10, Front. Endocrinol. 9 (2018) 524, https://doi.org/10.3389/fendo.2018.00524. PubMed PMID: 30298051; PubMed Central PMCID: PMCPMC6160580.

[10] S.K. Choi, M. Galán, M. Kassan, M. Partyka, M. Trebak, K. Matrougui, Poly(ADP-ribose) polymerase 1 inhibition improves coronary arteriole function in type 2 diabetes mellitus, Epub 2012/03/29, Hypertension 59 (5) (2012) 1060–1068, https://doi.org/10.1161/hypertensionaha.111.190140. PubMed PMID: 22454481; PubMed Central PMCID: PMCPMC3331962.

[11] W.L. Kraus, M.O. Hottiger, PARP-1 and gene regulation: progress and puzzles, Mol. Aspect. Med. 34 (6) (2013) 1109–1123, https://doi.org/10.1016/j.mam.2013.01.005. PubMed PMID: 23357755.

[12] H.E. Bryant, E. Petermann, N. Schultz, A.S. Jemth, O. Loseva, N. Issaeva, et al., PARP is activated at stalled forks to mediate Mre11-dependent replication restart and recombination, EMBO J. 28 (17) (2009) 2601–2615, https://doi.org/10.1038/emboj.2009.206. PubMed PMID: 19629035; PubMed Central PMCID: PMC2738702.

[13] Y.D. Zheng, X.Q. Xu, F. Peng, J.Z. Yu, H. Wu, The poly(ADP-ribose) polymerase-1 inhibitor 3-aminobenzamide suppresses cell growth and migration, enhancing suppressive effects of cisplatin in osteosarcoma cells, Oncol. Rep. 25 (5) (2011) 1399–1405, https://doi.org/10.3892/or.2011.1212. PubMed PMID: 21399878.

[14] I.U. Schraufstatter, P.A. Hyslop, D.B. Hinshaw, R.G. Spragg, L.A. Sklar, C. G. Cochrane, Hydrogen peroxide-induced injury of cells and its prevention by inhibitors of poly(ADP-ribose) polymerase, Proc. Natl. Acad. Sci. U. S. A 83 (13) (1986) 4908–4912. PubMed PMID: 2941760; PubMed Central PMCID: PMC323853.

[15] C. Szabo, B. Zingarelli, M. O'Connor, A.L. Salzman, DNA strand breakage, activation of poly (ADP-ribose) synthetase, and cellular energy depletion are involved in the cytotoxicity of macrophages and smooth muscle cells exposed to peroxynitrite, Proc. Natl. Acad. Sci. U. S. A 93 (5) (1996) 1753–1758. PubMed PMID: 8700830; PubMed Central PMCID: PMC39853.

[16] P. Pacher, C. Szabo, Role of poly(ADP-ribose) polymerase-1 activation in the pathogenesis of diabetic complications: endothelial dysfunction, as a common underlying theme, Antioxidants Redox Signal. 7 (11–12) (2005) 1568–1580, https://doi.org/10.1089/ars.2005.7.1568. PubMed PMID: 16356120; PubMed Central PMCID: PMC2228261.

[17] C. Szabo, A. Zanchi, K. Komjati, P. Pacher, A.S. Krolewski, W.C. Quist, et al., Poly (ADP-Ribose) polymerase is activated in subjects at risk of developing type 2 diabetes and is associated with impaired vascular reactivity, Circulation 106 (21) (2002) 2680–2686. PubMed PMID: 12438293.

[18] K. Oumouna-Benachour, C.P. Hans, Y. Suzuki, A. Naura, R. Datta, S. Belmadani, et al., Poly(ADP-ribose) polymerase inhibition reduces atherosclerotic plaque size and promotes factors of plaque stability in apolipoprotein E-deficient mice: effects on macrophage recruitment, nuclear factor-kappaB nuclear translocation, and foam cell death, Epub 2007/04/18, Circulation 115 (18) (2007) 2442–2450, https://doi.org/10.1161/circulationaha.106.668756. PubMed PMID: 17438151.

[19] C. Zhang, J. Yang, L.K. Jennings, Attenuation of neointima formation through the inhibition of DNA repair enzyme PARP-1 in balloon-injured rat carotid artery, Am. J. Physiol. Heart Circ. Physiol. 287 (2) (2004) H659–H666, https://doi.org/10.1152/ajpheart.00162.2004. PubMed PMID: 15044192.

[20] L.L. Zhai, Y. Wu, D.W. Huang, Z.G. Tang, Increased matrix metalloproteinase-2 expression and reduced tissue factor pathway inhibitor-2 expression correlate with angiogenesis and early postoperative recurrence of pancreatic carcinoma, Am. J. Tourism Res. 7 (11) (2015) 2412–2422. PubMed PMID: 26807187; PubMed Central PMCID: PMC4697719.

[21] C.N. Rao, S. Mohanam, A. Puppala, J.S. Rao, Regulation of ProMMP-1 and ProMMP-3 activation by tissue factor pathway inhibitor-2/matrix-associated serine protease inhibitor, Biochem. Biophys. Resear. Commun. 255 (1) (1999) 94–98, https://doi.org/10.1006/bbrc.1999.0153. PubMed PMID: 10082661.

[22] D. Kong, D. Ma, H. Bai, H. Guo, X. Cai, W. Mo, et al., Expression and characterization of the first kunitz domain of human tissue factor pathway

inhibitor-2, Biochem. Biophys. Resear. Commun. 324 (4) (2004) 1179–1185, https://doi.org/10.1016/j.bbrc.2004.09.179. PubMed PMID: 15504338.
[23] B. Zhao, X. Luo, H. Shi, D. Ma, Tissue factor pathway inhibitor-2 is downregulated by ox-LDL and inhibits ox-LDL induced vascular smooth muscle cells proliferation and migration, Thromb. Res. 128 (2) (2011) 179–185, https://doi.org/10.1016/j.thromres.2011.02.025. PubMed PMID: 21458846.
[24] M.P. Herman, G.K. Sukhova, W. Kisiel, D. Foster, M.R. Kehry, P. Libby, et al., Tissue factor pathway inhibitor-2 is a novel inhibitor of matrix metalloproteinases with implications for atherosclerosis, J. Clin. Invest. 107 (9) (2001) 1117–1126, https://doi.org/10.1172/JCI10403. PubMed PMID: 11342575; PubMed Central PMCID: PMC209273.
[25] H. Izumi, C. Takahashi, J. Oh, M. Noda, Tissue factor pathway inhibitor-2 suppresses the production of active matrix metalloproteinase-2 and is down-regulated in cells harboring activated ras oncogenes, Epub 2000/09/14, FEBS Lett. 481 (1) (2000) 31–36, https://doi.org/10.1016/s0014-5793(00)01902-5. PubMed PMID: 10984610.
[26] J. Ekstrand, A. Razuvaev, L. Folkersen, J. Roy, U. Hedin, Tissue factor pathway inhibitor-2 is induced by fluid shear stress in vascular smooth muscle cells and affects cell proliferation and survival, J. Vasc. Surg. 52 (1) (2010) 167–175, https://doi.org/10.1016/j.jvs.2010.02.282. PubMed PMID: 20537494.
[27] T. Higashikata, M. Yamagishi, T. Higashi, I. Nagata, K. Iihara, S. Miyamoto, et al., Altered expression balance of matrix metalloproteinases and their inhibitors in human carotid plaque disruption: results of quantitative tissue analysis using real-time RT-PCR method, Atherosclerosis 185 (1) (2006) 165–172, https://doi.org/10.1016/j.atherosclerosis.2005.05.039. PubMed PMID: 16039658.
[28] C. Zawadzki, N. Chatelain, M. Delestre, S. Susen, B. Quesnel, F. Juthier, et al., Tissue factor pathway inhibitor-2 gene methylation is associated with low expression in carotid atherosclerotic plaques, Atherosclerosis 204 (2) (2009) e4–14, https://doi.org/10.1016/j.atherosclerosis.2008.10.009. PubMed PMID: 19081094.
[29] A. Kumar, V. Lindner, Remodeling with neointima formation in the mouse carotid artery after cessation of blood flow, Epub 1997/11/14, Arterioscler. Thromb. Vasc. Biol. 17 (10) (1997) 2238–2244, https://doi.org/10.1161/01.atv.17.10.2238. PubMed PMID: 9351395.
[30] N. Nalabothula, T. Al-jumaily, A.M. Eteleeb, R.M. Flight, S. Xiaorong, H. Moseley, et al., Genome-wide profiling of PARP1 reveals an interplay with gene regulatory regions and DNA methylation, Epub 2015/08/26, PloS One 10 (8) (2015), e0135410, https://doi.org/10.1371/journal.pone.0135410. PubMed PMID: 26305327; PubMed Central PMCID: PMCPMC4549251.
[31] X. Xiao, X. Tao, Y. Wang, L. Zhu, Y. Ye, H. Liu, et al., Hypomethylation of tissue factor pathway inhibitor 2 in human placenta of preeclampsia, Thromb. Res. 152 (2017) 7–13, https://doi.org/10.1016/j.thromres.2017.02.005. PubMed PMID: 28208084.
[32] Q. Zhang, Y. Zhang, S.Z. Wang, N. Wang, W.G. Jiang, Y.H. Ji, et al., Reduced expression of tissue factor pathway inhibitor-2 contributes to apoptosis and angiogenesis in cervical cancer, J. Exp. Clin. Canc. Res. : CR (Clim. Res.) 31 (2012) 1, https://doi.org/10.1186/1756-9966-31-1. PubMed PMID: 22208663; PubMed Central PMCID: PMC3314549.
[33] P.A. Jones, S.B. Baylin, The fundamental role of epigenetic events in cancer, Nat. Rev. Genet. 3 (6) (2002) 415–428, https://doi.org/10.1038/nrg816. PubMed PMID: 12042769.
[34] F. Giacco, M. Brownlee, Oxidative stress and diabetic complications, Epub 2010/10/30, Circ. Res. 107 (9) (2010) 1058–1070, https://doi.org/10.1161/circresaha.110.223545. PubMed PMID: 21030723; PubMed Central PMCID: PMCPMC2996922.
[35] T. El-Hamoly, C. Hegedus, P. Lakatos, K. Kovacs, P. Bai, M.A. El-Ghazaly, et al., Activation of poly(ADP-ribose) polymerase-1 delays wound healing by regulating keratinocyte migration and production of inflammatory mediators, Mol. Med. 20 (2014) 363–371, https://doi.org/10.2119/molmed.2014.00130. PubMed PMID: 25014793; PubMed Central PMCID: PMC4153841.
[36] M.M. Rosado, E. Bennici, F. Novelli, C. Pioli, Beyond DNA repair, the immunological role of PARP-1 and its siblings, Immunology 139 (4) (2013) 428–437, https://doi.org/10.1111/imm.12099. PubMed PMID: 23489378; PubMed Central PMCID: PMC3719060.
[37] M.I. Rodríguez, A. Peralta-Leal, F. O'Valle, J.M. Rodriguez-Vargas, A. Gonzalez-Flores, J. Majuelos-Melguizo, et al., PARP-1 regulates metastatic melanoma through modulation of vimentin-induced malignant transformation, Epub 2013/06/21, PLoS Genet. 9 (6) (2013), e1003531, https://doi.org/10.1371/journal.pgen.1003531. PubMed PMID: 23785295; PubMed Central PMCID: PMCPMC3681683.
[38] K. Shahzad, M. Thati, H. Wang, M. Kashif, J. Wolter, S. Ranjan, et al., Minocycline reduces plaque size in diet induced atherosclerosis via p27(Kip1), Epub 2011/07/02, Atherosclerosis 219 (1) (2011) 74–83, https://doi.org/10.1016/j.atherosclerosis.2011.05.041. PubMed PMID: 21719015.
[39] J. Pan, D. Ma, F. Sun, W. Liang, R. Liu, W. Shen, et al., Over-expression of TFPI-2 promotes atherosclerotic plaque stability by inhibiting MMPs in apoE-/- mice, Epub 2013/04/24, Int. J. Cardiol. 168 (2) (2013) 1691–1697, https://doi.org/10.1016/j.ijcard.2013.03.073. PubMed PMID: 23608390.
[40] C. Xu, H. Wang, H. He, F. Zheng, Y. Chen, J. Zhang, et al., Low expression of TFPI-2 associated with poor survival outcome in patients with breast cancer, BMC Canc. 13 (2013) 118, https://doi.org/10.1186/1471-2407-13-118. PubMed PMID: 23497249; PubMed Central PMCID: PMC3607852.
[41] G. Wang, Y. Zeng, S. Chen, D. Li, W. Li, Y. Zhou, et al., Localization of TFPI-2 in the nucleus modulates MMP-2 gene expression in breast cancer cells, Sci. Rep. 7 (1) (2017) 13575, https://doi.org/10.1038/s41598-017-14148-8. PubMed PMID: 29051606; PubMed Central PMCID: PMC5648759.
[42] J. Hong, R. Liu, L. Chen, B. Wu, J. Yu, W. Gao, et al., Conditional knockout of tissue factor pathway inhibitor 2 in vascular endothelial cells accelerates atherosclerotic plaque development in mice, Epub 2015/11/26, Thromb. Res. 137 (2016) 148–156, https://doi.org/10.1016/j.thromres.2015.11.010. PubMed PMID: 26603320.
[43] J.T. Crawley, D.A. Goulding, V. Ferreira, N.J. Severs, F. Lupu, Expression and localization of tissue factor pathway inhibitor-2 in normal and atherosclerotic human vessels, Epub 2002/02/09, Arterioscler. Thromb. Vasc. Biol. 22 (2) (2002) 218–224, https://doi.org/10.1161/hq0102.101842. PubMed PMID: 11834519.
[44] A. Koch, S.C. Joosten, Z. Feng, T.C. de Ruijter, M.X. Draht, V. Melotte, et al., Analysis of DNA methylation in cancer: location revisited, Epub 2018/04/19, Nat. Rev. Clin. Oncol. 15 (7) (2018) 459–466, https://doi.org/10.1038/s41571-018-0004-4. PubMed PMID: 29666440.
[45] G. Wang, W. Huang, W. Li, S. Chen, W. Chen, Y. Zhou, et al., TFPI-2 suppresses breast cancer cell proliferation and invasion through regulation of ERK signaling and interaction with actinin-4 and myosin-9, Sci. Rep. 8 (1) (2018) 14402, https://doi.org/10.1038/s41598-018-32698-3. PubMed PMID: 30258071; PubMed Central PMCID: PMC6158255.